

# Spin dynamics of the one-dimensional double chain spin- $\frac{1}{2}$ antiferromagnet KNaCuP<sub>2</sub>O<sub>7</sub>

Ganesan Senthil Murugan<sup>1,2,\*</sup>, Suheon Lee,<sup>3,\*</sup> C. Wang,<sup>4</sup> H. Luetkens,<sup>4</sup> Kwang-Yong Choi<sup>5,†</sup>, and Raman Sankar<sup>2,‡</sup>

<sup>1</sup>Center for Condensed Matter Sciences, National Taiwan University, Taipei 10617, Taiwan

<sup>2</sup>Institute of Physics, Academia Sinica, Nankang, Taipei 11529, Taiwan

<sup>3</sup>Center for Integrated Nanostructure Physics, Institute for Basic Science (IBS), Suwon 16419, Republic of Korea

<sup>4</sup>Laboratory for Muon Spin Spectroscopy, Paul Scherrer Institute, 5232 Villigen, Switzerland

<sup>5</sup>Department of Physics, Sungkyunkwan University, Suwon 16419, Republic of Korea



(Received 12 March 2022; revised 2 May 2022; accepted 19 May 2022; published 31 May 2022)

We combine a muon spin relaxation ( $\mu$ SR) technique with thermodynamic measurements to explore the spin dynamics of one-dimensional (1D)  $S = \frac{1}{2}$  antiferromagnetic double chain KNaCuP<sub>2</sub>O<sub>7</sub>. Static magnetic susceptibility and specific heat are well described by a uniform 1D spin chain model with the intrachain interaction  $J/k_B \approx 55$  K and small interchain interactions. Spin excitations probed by zero-field  $\mu$ SR evince that high-temperature diffusive spin transport turns into ballistic behavior with decreasing temperature below 30 K. In addition, we observe that longitudinal-field  $\mu$ SR varies hardly with an external magnetic field. The field-independent dynamical spin susceptibility disagrees with diffusive or ballistic behaviors.

DOI: [10.1103/PhysRevB.105.174442](https://doi.org/10.1103/PhysRevB.105.174442)

## I. INTRODUCTION

Since the pioneering works of Ising and Bethe [1,2], one-dimensional (1D) spin chains have been the subject of continuous theoretical and experimental research. 1D quantum magnets host ground states and phases markedly different from their higher-dimensional counterparts and provide a conspicuous laboratory to examine fundamental theories of quantum magnetism due to their analytical solvability [3].

A  $S = \frac{1}{2}$  antiferromagnetic Heisenberg spin chain (AFHC) is known to harbor a spin-liquid ground state even in the limit of zero temperature, in which reduced dimensionality and strong quantum fluctuations inhibit long-range order despite the algebraically decaying spin-spin correlations [4]. As local excitations do not exist in one dimension, a spin-flip excitation is fractionalized into spinons carrying spin- $\frac{1}{2}$  without charge [5]. Noticeably, a nontrivial crossover occurs between the high-temperature superdiffusive regime and the low-temperature response described by the Tomonaga-Luttinger liquid (TLL) theory, which predicts power-law spin correlations or fractionalization of the excitations [6–13]. Owing to the integrability of a  $S = \frac{1}{2}$  AFHC, ballistic spin transport is purported to dictate dynamic properties of finite magnetic fields and a ground state [14,15].

From a material perspective, experimental realizations of a true 1D quantum spin chain are challenging as residual, nonfrustrated interchain couplings are apt to stabilize a long-range magnetic order. Notwithstanding, inherent 1D physics is still retained in the presence of weak interchain interactions. Among  $S = \frac{1}{2}$  spin chain compounds, copper-based oxides

(Cu<sup>2+</sup>; 3d<sup>9</sup>) provide a rich reservoir for AFHC model systems due to their versatile connectivity of exchange paths.

The prominent instances include CuGeO<sub>3</sub> [16], SrCuO<sub>2</sub> [17], Sr<sub>2</sub>CuO<sub>3</sub> [17], LiCuVO<sub>4</sub> [18], Li<sub>2</sub>CuO<sub>2</sub> [19,20],  $\gamma$ -LiV<sub>2</sub>O<sub>5</sub> [21], and Cs<sub>4</sub>CuSb<sub>2</sub>Cl<sub>12</sub> [22]. In particular, the copper phosphates (Sr, Ba)<sub>2</sub>Cu(PO<sub>4</sub>)<sub>2</sub> [23,24], (Sr, Pb)CuP<sub>2</sub>O<sub>7</sub> [25], BaCuP<sub>2</sub>O<sub>7</sub> [26], K<sub>2</sub>CuP<sub>2</sub>O<sub>7</sub> [27], and (Li, Na)<sub>2</sub>CuP<sub>2</sub>O<sub>7</sub> [28] have been regarded as the best realization of a uniform 1D Heisenberg chain. This is owed to the fact that individual chains formed by the corner/edge sharing of CuO<sub>4</sub> and PO<sub>4</sub> tetrahedra are separated by the alkali cations.

Herein, we focus on KNaCuP<sub>2</sub>O<sub>7</sub>, which belongs to the family of A<sub>2</sub>CuP<sub>2</sub>O<sub>7</sub> (A = Na, Li, and K) [29]. KNaCuP<sub>2</sub>O<sub>7</sub> crystallizes in a monoclinic structure with space group P21/n, which is distinct from its sister compounds: (Na, Li)<sub>2</sub>Cu<sub>2</sub>O<sub>7</sub> with space group C2/c and K<sub>2</sub>Cu<sub>2</sub>O<sub>7</sub> with space group Pbnm. As depicted in Fig. 1(a), distorted CuO<sub>4</sub> plaquettes are connected by four corner-sharing PO<sub>4</sub> tetrahedra, forming spin chains with the intrachain exchange coupling  $J$  along the  $a$  axis. The Na and K alkali cations are located in the interstitial sites between two neighboring chains, giving rise to frustrated interchain couplings. The interchain couplings  $J'$  and  $J''$  are much smaller than the intrachain interaction  $J$  due to the large interchain distance (5.676–5.772 Å). Recent <sup>31</sup>P and <sup>23</sup>Na nuclear magnetic resonance (NMR) and thermodynamic studies in conjunction with first-principles calculations show that KNaCuP<sub>2</sub>O<sub>7</sub> realizes a quasi-1D uniform  $S = \frac{1}{2}$  Heisenberg antiferromagnet with  $J/k_B \simeq 58.7$  K [30]. Magnetic long-range order was precluded down to 2 K, supporting the notion of weak, frustrated interchain couplings.

In this paper, we employ muon spin relaxation ( $\mu$ SR) and thermodynamic measurements to clarify whether low-energy spin excitations of KNaCuP<sub>2</sub>O<sub>7</sub> bear spin dynamics inherent to a  $S = \frac{1}{2}$  AFHC model. A temperature dependence of low-energy dynamical susceptibility obtained from the

\*These authors contributed equally to this work.

†Corresponding author: choisky99@skku.edu

‡Corresponding author: sankarndf@gmail.com

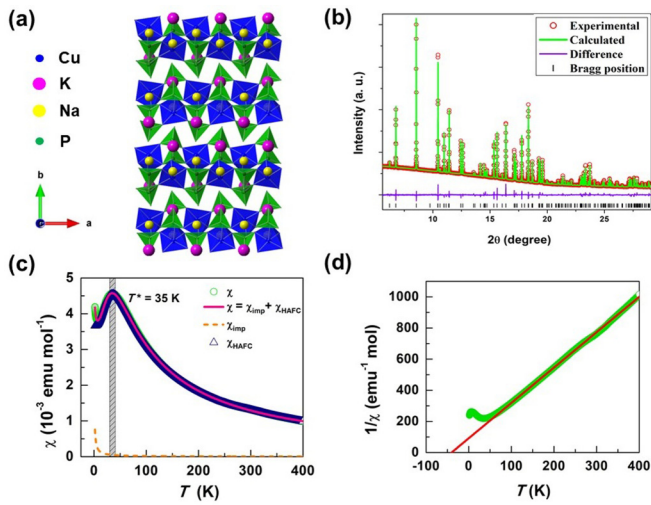


FIG. 1. (a) Crystal structure of KNaCuP<sub>2</sub>O<sub>7</sub>. The Cu atoms (blue balls) constitute a double chain formed by the corrugated layer of corner-shared CuO<sub>5</sub> distorted square pyramids bridged by P<sub>2</sub>O<sub>7</sub> groups along the *a* direction. The alkali cations (pink and yellow spheres) are located in the interstitial sites between the layers. (b) Rietveld refinement of the synchrotron XRD powder pattern of KNaCuP<sub>2</sub>O<sub>7</sub> taken at room temperature. The observed data, Rietveld refinement fit, difference curve, and Bragg peaks are denoted by the red open circles, green solid line, purple line, and vertical black dashes, respectively. (c) Temperature dependence of the dc magnetic susceptibility  $\chi(T)$  of KNaCuP<sub>2</sub>O<sub>7</sub> measured in an applied field of  $\mu_0 H = 0.01$  T. The pink solid line represents a fit to Eq. (1). The dc magnetic susceptibility is composed of the impurity contribution  $\chi_{\text{imp}}$  (orange dashed curve) and the Heisenberg antiferromagnetic spin chain susceptibility  $\chi_{\text{chain}}$  (open triangle symbol). (d) Inverse magnetic susceptibility  $1/\chi$  as a function of temperature. The red solid line is the Curie-Weiss law fit of the  $T = 150$ – $300$  K data to  $\chi(T) \sim C/(T - \Theta_{\text{CW}})$ .

muon spin-lattice relaxation rate demonstrates a diffusive-to-ballistic crossover of spin transport on cooling through 30 K. Conversely, a magnetic-field dependence of the dynamic susceptibility lacks signatures of 1D spin dynamics, deserving of further investigations.

## II. EXPERIMENTAL DETAILS

A polycrystalline sample of KNaCuP<sub>2</sub>O<sub>7</sub> was synthesized by the standard solid-state reaction method with a stoichiometric amount of K<sub>2</sub>CO<sub>3</sub>, Na<sub>2</sub>CO<sub>3</sub>, CuO, and P<sub>2</sub>O<sub>5</sub> (purity higher than 99.95%). The mixture of reagents was heated at 400 °C for 48 h in air, ground, and sintered at 500 and 570 °C for 48 h each with intermediate grindings.

The phase purity and crystal structure were checked by synchrotron x-ray diffraction (XRD) using the MYTHEN detector with a 15 keV beam at 09A beamline of NSRRC in Taiwan. The powder sample was packed in a 0.1-mm borosilicate capillary tube. The capillary tube was kept spinning during the data collection. The data were analyzed by the Rietveld method using the Bruker TOPAS program. Figure 1(b) shows the synchrotron powder XRD pattern of KNaCuP<sub>2</sub>O<sub>7</sub> measured at room temperature. The refined lattice parameters are  $a = 5.18610 \pm 0.00002$  Å,

$b = 14.00281 \pm 0.00005$  Å,  $c = 9.08173 \pm 0.00003$  Å, and  $V = 659.344 \pm 0.004$  Å<sup>3</sup>, which are in good agreement with the values reported in the literature [29]. The goodness of fit obtained by the residual refinement factors is  $R_p = 1.36\%$ ,  $R_{wp} = 2.23\%$ ,  $R_{exp} = 0.39\%$ , and  $\chi^2 = 5.78$ .

Magnetic susceptibility was measured using a superconducting quantum interference device vibrating-sample magnetometer (SQUID-VSM, Quantum Design). The specific heat measurements were performed using a standard relaxation method with a physical property measurement system (PPMS, Quantum Design). Muon spin relaxation ( $\mu$ SR) experiments were performed on the GPS spectrometer at Paul Scherrer Institute (Villigen, Switzerland). The finely ground polycrystalline samples of KNaCuP<sub>2</sub>O<sub>7</sub> were packed using an alumina foil and attached to the sample holder. The detector efficiency between forward and backward positron detectors was determined from the weak transverse field measurements in an applied field of  $H = 50$  G at 200 K. All the  $\mu$ SR data were analyzed using the MUSRFIT software package [31].

## III. RESULTS AND DISCUSSION

### A. Magnetic susceptibility and specific heat

In Fig. 1(c), we present the temperature dependence of the dc magnetic susceptibilities  $\chi(T)$  ( $=M/H$ ) of KNaCuP<sub>2</sub>O<sub>7</sub> measured in an applied field of  $\mu_0 H = 0.01$  T. We observe no thermal hysteresis between the zero-field-cooled (ZFC) and field-cooled (FC) cycles, ruling out the presence of inhomogeneous magnetism.  $\chi(T)$  shows a broad maximum at  $T^* = 35$  K, characteristic of low-dimensional systems featuring short-range ordering. For temperatures below 6.5 K, a Curie-like upturn arises from paramagnetic impurities and defect spins. We detect no signature of long-range magnetic ordering down to 1.8 K.

We first analyze the high-*T* paramagnetic  $\chi(T)$  data ( $T = 150$ – $300$  K) in terms of the Curie-Weiss law  $\chi(T) \sim C/(T - \Theta_{\text{CW}})$ . We obtain the Curie constant  $C = 0.4402 \pm 0.0003$  emu mol<sup>-1</sup> K and the Curie-Weiss temperature  $\Theta_{\text{CW}} = -40.21 \pm 0.93$  K [see the red solid line in the inset of Fig. 1(d)]. The negative  $\Theta_{\text{CW}}$  value indicates the dominant antiferromagnetic couplings between the adjacent Cu<sup>2+</sup> spins. The calculated effective magnetic moment of  $\mu_{\text{eff}} = 1.87 \pm 0.02\mu_B$  per Cu<sup>2+</sup> from the Curie constant is slightly larger than the spin- $\frac{1}{2}$  only value of  $\mu_{\text{cal}} = 1.73\mu_B$ . Here,  $\mu_B$  is the Bohr magneton. In order to differentiate between the impurity  $\chi_{\text{imp}}$  and spin chain  $\chi_{\text{chain}}$  contributions, the observed  $\chi_{\text{tot}}(T)$  data are modeled with the following expression,

$$\chi_{\text{tot}}(T) = \chi_0 + \chi_{\text{imp}}(T) + \chi_{\text{chain}}(T), \quad (1)$$

where  $\chi_0$  is the temperature-independent susceptibility which includes the Van Vleck paramagnetic and core diamagnetic contributions.  $\chi_{\text{imp}} = C_{\text{imp}}/(T - \Theta_{\text{imp}})$  captures a paramagnetic impurity contribution, and  $\chi_{\text{chain}}(T)$  is the  $S = \frac{1}{2}$  uniform antiferromagnetic chain model calculated by Johnston *et al.* [32]. Here,  $C_{\text{imp}}$  and  $\Theta_{\text{imp}}$  are the Curie constant and Curie-Weiss temperature for impurity spins, respectively. Optimized fittings of the  $\chi_{\text{tot}}(T)$  data yield  $\chi_0 = (1.40 \pm 0.23) \times 10^{-5}$  emu/mol,  $C_{\text{imp}} = 0.0017 \pm 0.0005$  emu mol<sup>-1</sup> K,  $\Theta_{\text{imp}} = -0.45 \pm 0.03$  K, the intrachain

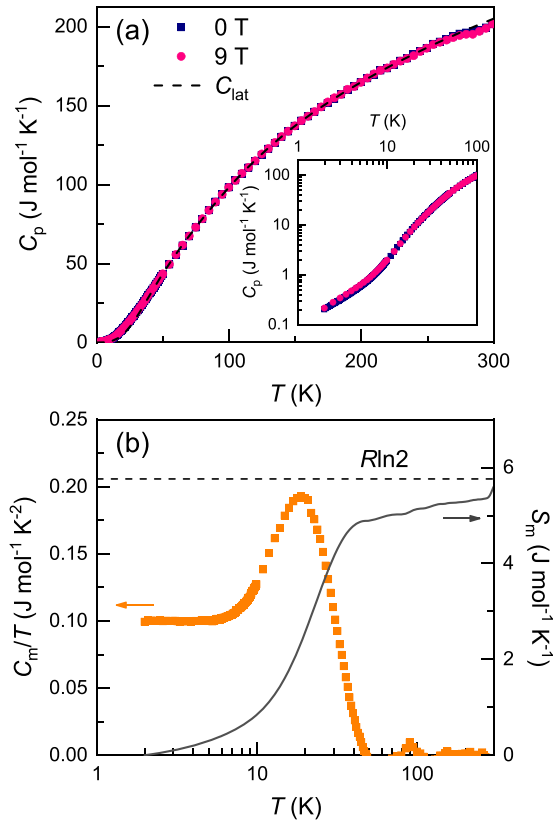


FIG. 2. (a) Temperature dependence of the total heat capacity  $C_p(T)$  in selected magnetic fields  $B = 0$  (pink solid circles) and  $9\text{ T}$  (indigo blue squares). The dashed curve denotes the evaluated lattice contributions using the combined Debye and Einstein model. The log-log plot of  $C_p(T)$  in the inset demonstrates no difference between  $\mu_0H = 0$  and  $9\text{ T}$ . (b) Temperature dependence of the magnetic specific heat divided by temperature  $C_m/T$  on a log scale. The solid line is the calculated spin entropy  $S_m(T)$  as a function of temperature.

interaction  $J/k_B \approx 55\text{ K}$ , and the  $g$  factor of  $g \approx 2.12$ . Overall, the extracted parameters are comparable to the reported values [30]. The impurity concentration is estimated to be 0.4%. The small value of  $\Theta_{\text{imp}}$  indicates that the impurity spins are weakly coupled. Further, we testify the validity of the  $S = \frac{1}{2}$  AFHC based on the relationship  $\chi(T = T^*)T^* = 0.0353g^2$ . With  $\chi(T = T^*) = 0.00455 \text{ emu mol}^{-1}$  and  $T^* = 35\text{ K}$ , we obtain  $\chi(T = T^*)T^*/g^2 = 0.03543$ , consistent with the theoretical value [32].

To probe low-energy quasiparticle excitations, we performed heat capacity measurements over the temperature range of  $T = 2\text{--}300\text{ K}$ . Figure 2(a) shows the specific heat as a function of temperature  $C_p(T)$  in zero magnetic field and  $\mu_0H = 9\text{ T}$ . No  $\lambda$ -type anomaly associated with the long-range magnetic order was seen down to 2 K. In addition, we find no essential difference between  $C_p(T, \mu_0H = 0\text{ T})$  and  $C_p(T, \mu_0H = 9\text{ T})$ , as seen from the inset of Fig. 2(a).

The magnetic specific heat  $C_m$  is singled out by subtracting the lattice contribution  $C_{\text{lat}}$  from the total heat capacity. We estimate the  $C_{\text{lat}}$  contribution by fitting of the  $C_p(T)$  data in the temperature range of  $T = 45\text{--}250\text{ K}$  using a sum of one Debye ( $C_{\text{Debye}}$ ) and two Einstein ( $C_{\text{Einstein},i}$ ) terms:

$C_{\text{lat}} = C_{\text{Debye}} + C_{\text{Einstein},i}$ . The  $C_{\text{Debye}}$  and  $C_{\text{Einstein},i}$  terms are given as

$$C_{\text{Debye}} = a \left[ 9R \left( \frac{T}{\theta_D} \right)^3 \int_0^{\theta_D/T} \frac{x^4 e^x}{(e^x - 1)^2} dx \right], \quad (2)$$

$$C_{\text{Einstein},i} = 3R \sum_{i=1}^2 b_i \left[ \left( \frac{\theta_{E,i}}{T} \right)^2 \frac{e^{\theta_{E,i}/T}}{(e^{\theta_{E,i}/T} - 1)^2} \right], \quad (3)$$

where  $R$  is the universal gas constant, and  $\theta_D$  and  $\theta_{E,i}$  are the Debye and Einstein temperatures, respectively. The  $a$  and  $b_i$  are the weighting factors of the Debye and Einstein coefficients, respectively. In the course of the fittings, the sum of oscillator strengths was fixed to match with the total number of atoms per the formula unit, namely,  $a + b_1 + b_2 = 12$ . With the fitting parameters  $\theta_D = 225.7(2)\text{ K}$ ,  $\theta_{E,1} = 483.9(7)\text{ K}$ ,  $\theta_{E,2} = 1300.4(9)\text{ K}$ ,  $a = 4.0(5)$ ,  $b_1 = 4.1(3)$ , and  $b_2 = 3.9(4)$ , we reach a good agreement between the experimental data and the theoretical calculation.

In Fig. 2(b), we plot the resulting magnetic specific heat divided by temperature  $C_m/T$  vs  $T$  on a log scale.  $C_m/T$  shows a broad maximum around 16 K and then nearly flattens out below 5 K. Further, we note that  $C_m/T$  is almost quenched above 50 K ( $\approx J/k_B$ ). The low- $T$  linear magnetic contribution  $C_m/T = \gamma$  is characteristic of a gapless 1D  $S = \frac{1}{2}$  AFHC, enabling estimation of  $J/k_B$  by the relation  $\gamma_{\text{th}} = 2\bar{R}/(3J/k_B)$  for  $T < 0.2J/k_B$  [32]. With  $J/k_B \approx 55\text{ K}$ , we evaluate  $\gamma = 0.0987(2) \text{ J mol}^{-1} \text{ K}^{-2}$ , in good agreement with the theoretical value of  $\gamma_{\text{th}} = 0.1 \text{ J mol}^{-1} \text{ K}^{-2}$ . The  $T$  dependence of the magnetic entropy  $S_m$ , calculated by integrating  $C_m/T$  over a temperature, is plotted in the right panel of Fig. 2(b). At paramagnetic high temperatures, the total magnetic entropy  $S_m(T)$  reaches  $5.59 \text{ J mol}^{-1} \text{ K}^{-1}$ , which is somewhat smaller than the theoretical value  $R \ln(2s+1) = 5.76 \text{ J mol}^{-1} \text{ K}^{-1}$  for  $S = \frac{1}{2}$ . The missing magnetic entropy heralds weak magnetic ordering for temperatures below 1 K, which should be confirmed by the future low- $T$  specific heat and  $\mu\text{SR}$  measurements. Thus, we did not attempt to make a linear extrapolation of  $C_{\text{lat}}$  down to zero.

## B. Muon spin relaxation

To investigate the slow-time behavior of local spin correlations inherent to the TLL phase, we conducted zero-field (ZF)- and longitudinal-field (LF)- $\mu\text{SR}$  experiments down to  $T = 1.6\text{ K}$ .

Shown in Fig. 3(a) are the ZF- $\mu\text{SR}$  spectra at selected temperatures. Over the entire measured temperature range of  $T = 1.6\text{--}200\text{ K}$ , the ZF- $\mu\text{SR}$  spectra are dominated by a Gaussian-like relaxation, while showing a small variation with temperature. The Gaussian relaxation shape is characteristic of quasistatic nuclear moments. Additionally, the quantum fluctuations of electronic moments give rise to an exponential relaxation of the muon spin polarization. The gross relaxation function is described by the Gaussian Kubo-Toyabe function  $G_{\text{KT}}(\Delta t)$  multiplied by a simple exponential function,  $P_z(t) = G_{\text{KT}} \exp(-\lambda_{\text{ZF}}t)$ . Here, the Gaussian Kubo-Toyabe function is given by  $G_{\text{KT}}(\Delta t) = \frac{1}{3} + \frac{2}{3}[1 - (\Delta t)^2] \exp[-\frac{1}{2}(\Delta t)^2]$ ,  $\lambda_{\text{ZF}}$  is the ZF muon spin relaxation rate, and  $\Delta$  is the nuclear field distribution [33]. None of the following signatures of long-range magnetic ordering were observed: (i) coherent muon

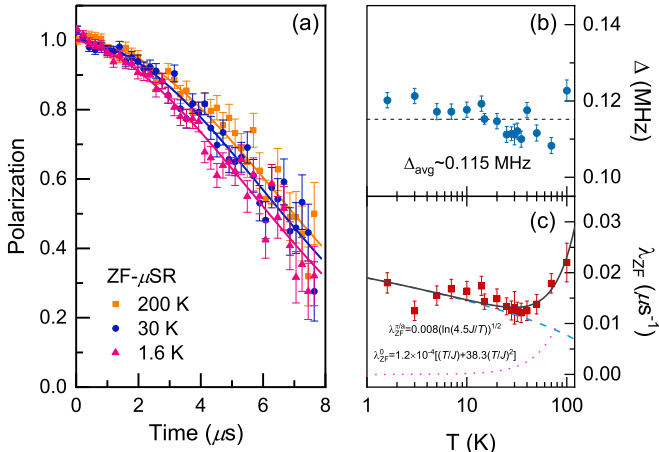


FIG. 3. (a) Representative ZF- $\mu$ SR spectra at various temperatures  $T = 1.6, 30$ , and  $200$  K. The solid curves denote the fits to the data using the Gaussian Kubo-Toyabe function multiplied by an exponential function. (b) Nuclear field distribution  $\Delta(T)$  as a function of temperature. The horizontal dashed line represents an average value of  $\Delta(T) \sim 0.115$  MHz. (c) Temperature dependence of the muon spin relaxation rate. The dotted and dashed curves indicate the contributions of the spin excitations from  $q = \pi/a$  and  $q = 0$ , as described in the main text.

spin oscillation signals, (ii) loss of initial asymmetry, and (iii)  $1/3$  recovery of the muon spin polarization. This observation is consistent with the previous NMR results, suggesting the long-range magnetic order around  $T_N \sim 1$  K [30].

The obtained fitting parameters are plotted in Figs. 3(b) and 3(c). The nuclear field distribution  $\Delta(T)$  is nearly temperature independent with an average value of  $\Delta \sim 0.115$  MHz. We find that the electronic contribution to the muon spin relaxation,  $\lambda_{ZF}$ , is roughly one order of magnitude smaller than  $\Delta$ , implying that the electronic moments rapidly fluctuate at all the measured temperatures. As shown in Fig. 3(c),  $\lambda_{ZF}(T)$  exhibits nonmonotonic behavior. Before proceeding, we recall that for the 1D  $S = \frac{1}{2}$  AFHC, the muon spin relaxation is composed of two contributions [34,35]: (i) uniform  $q = 0$  spin excitations and (ii) staggered  $q = \pi/a$  excitations. The uniform contribution leads to  $\lambda_{ZF}(T) \sim T/J + 38.3(T/J)^2$  [see the dotted line in Fig. 3(c)], while the staggered component gives a  $\sqrt{\ln(4.5J/T)}$  dependence [see the dashed line in Fig. 3(c)]. Our  $\lambda_{ZF}(T)$  data are best reproduced by a sum of the  $q = 0$  and  $q = \pi/a$  contributions [see the solid line in Fig. 3(c)]. This analysis reveals that the muon relaxation rate is dominated by the  $q = 0$  ( $q = \pi/a$ ) term above  $T = 30$  K (below  $T = 30$  K). The essentially same trend is observed by  $\mu$ SR of DEOCC-TCNQF<sub>4</sub> [36] and <sup>23</sup>Na NMR of the studied compound [30]. Consistent with our  $\mu$ SR results, <sup>23</sup>Na  $1/T_1$  shows the switching of the dominant contribution from the high- $T$  uniform to the low- $T$  staggered excitations through  $T \approx 20\text{--}30$  K [30].

To shine a light on the nature of spin transport and spin-spin correlation, we turn to the LF- $\mu$ SR results of KNaCuP<sub>2</sub>O<sub>7</sub>. Figure 4 presents the selected LF- $\mu$ SR measured at  $T = 1.6$  K and  $T = 70$  K. Apparently, a small applied LF (<10 G) can decouple the muon spins from the internal nuclear fields. However, in the applied LF of 100 G, we observe a small but

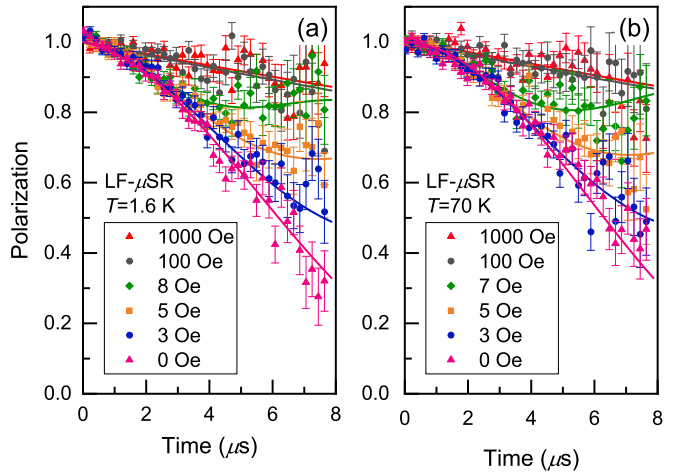


FIG. 4. Representative LF- $\mu$ SR spectra at (a)  $T = 1.6$  K and (b)  $T = 70$  K. The solid curves indicate the fits to the data using the Gaussian Kubo-Toyabe function in a longitudinal external field multiplied by an exponential function.

finite relaxation, suggesting the residual dynamically fluctuating spins.

The LF data are well described by the Gaussian Kubo-Toyabe function in an external LF multiplied by an exponential function,  $P_z(t) = G_{KT}^{\text{LF}} \exp(-\lambda_{\text{LF}}t)$ . Here,  $G_{KT}^{\text{LF}}$  is the Gaussian Kubo-Toyabe function in an applied LF,  $G_{KT}^{\text{LF}} = 1 - \frac{2\Delta^2}{(2\pi\nu_{\text{LF}})^2} [1 - \exp(-\frac{1}{2}\Delta^2 t^2) \cos(2\pi\nu_{\text{LF}}t)] + \frac{2\Delta^4}{(2\pi\nu_{\text{LF}})^3} \int_0^t \exp(-\frac{1}{2}\Delta^2 \tau^2) \sin(2\pi\nu_{\text{LF}}\tau) d\tau$ , where  $\nu_{\text{LF}}$  is the frequency of an applied LF [37]. All the data are well fitted with the common value of  $\Delta = 0.120(2)$  MHz, corresponding to the local field  $\sim 8.85$  G. This is well consistent with the nearly decoupled LF data at 100 G, which is typically ten times larger than the internal random static fields.

In Fig. 5, we exhibit the field dependence of the longitudinal relaxation rate  $\lambda_{\text{LF}}(H)$ . The steep increase of  $\lambda_{\text{LF}}(H)$  below 10 G is ascribed to decoupling the muon spins from the nuclear dipole field distribution. For applied fields above 10 G, the field dependence of  $\lambda_{\text{LF}}(H)$  is largely dominated by fluctuations of the local electronic magnetic fields and becomes nearly  $H$  independent.

In a  $S = \frac{1}{2}$  AFHC, three different types of spin transport have been discussed: diffusive, ballistic, and superdiffusive. Fluctuations at  $q = 0$  are diffusive at high temperatures and ballistic in the low- $T$  TLL regime [34]. In contrast, fluctuations at  $q = \pi/a$  are diffusive, yet ballistic as  $q$  is off from this point. The spectral density varies with frequency  $\omega$  as  $f(\omega) \sim \ln(J/\omega)$  for ballistic motion and  $f(\omega) \sim \omega^{-1/2}$  for 1D diffusive transport. Accordingly, the  $H$  dependence of  $\lambda_{\text{LF}}$  follows  $1/\sqrt{H}$  behavior for 1D diffusion (the dashed lines in Fig. 5) and  $\ln(J/H)$  for ballistic spin transport (the dotted lines in Fig. 5). This theoretical prediction has been observed in a number of  $\mu$ SR and NMR studies on  $S = \frac{1}{2}$  AFHC compounds including SrCuO<sub>2</sub>, Sr<sub>2</sub>CuO<sub>3</sub>, Rb<sub>4</sub>Cu(MoO<sub>4</sub>)<sub>3</sub>, and DEOCC-TCNQF<sub>4</sub> [36,38–40]. On the other hand, a series of recent theoretical calculations have established that the high- $T$  dynamics of the  $S = \frac{1}{2}$  AFHC obeys the

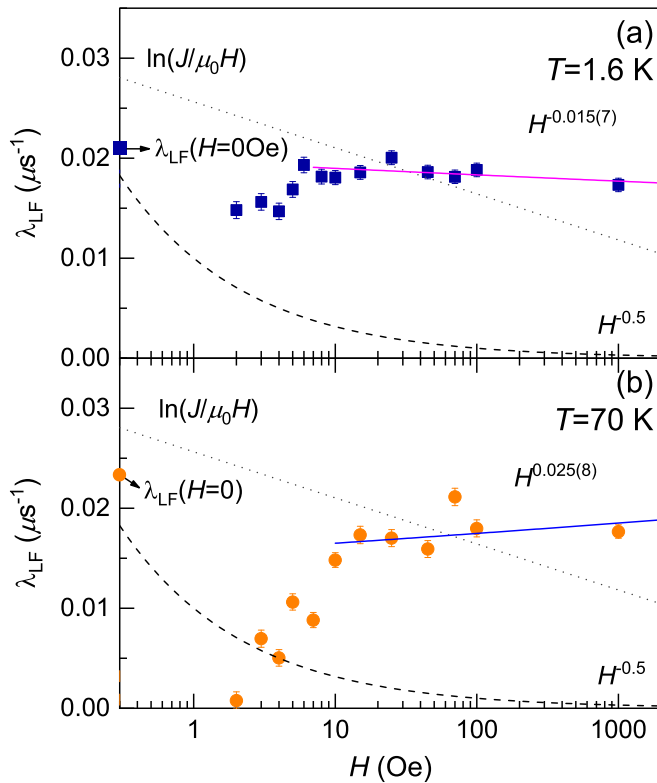


FIG. 5. Longitudinal-field dependence of the muon spin relaxation rate  $\lambda_{\text{LF}}(H)$  measured at (a)  $T = 1.6$  K and (b)  $T = 70$  K. The dotted line illustrates the logarithmic behavior expected for ballistic spin transport. The dashed line denotes a spin diffusion model. The solid lines indicate the power-law behaviors  $\lambda_{\text{LF}} \sim T^n$ .

Kardar-Parisi-Zhang (KPZ) universality class with the dynamical exponent  $z = 3/2$  and that a spatiotemporal crossover occurs from a high- $T$  superdiffusive regime related to KPZ hydrodynamics to low- $T$  ballistic dynamics [9–13,41]. The predicted superdiffusive behavior was confirmed in  $\text{KCuF}_3$  by inelastic scattering in the limit of small momentum and vanishing frequency [42]. So far, however,  $\mu\text{SR}$  and NMR evidence for the superdiffusive transport is lacking.

Analysis of our  $\lambda_{\text{LF}}(H)$  data reveals that no known theoretical models can provide a description of both the low-

and high- $T$  data (compare the theoretical curves with the experimental data). At the moment, it is not far clear why the  $H$  dependence of  $\lambda_{\text{LF}}(H)$  is neither (super)diffusive nor ballistic. One thinkable origin is impurities, which can modify a low-energy excitation spectrum, as inferred from the Curie tail of  $\chi(T)$  in Fig. 1(c). Given the fact that the  $T$ -dependence  $\lambda_{\text{ZF}}$  contains the  $q = 0$  and  $q = \pi/a$  excitations, a small amount of impurities can admix these two modes and allow for additional contributions arising from  $q \neq 0, \pi/a$  excitations [36]. In addition to the impurity-induced localized excitations, quadrupolar resonances arising from three quadrupolar nuclei present in this material could also increase the observed relaxation rate relative to the expected behaviors. Future experiments in higher fields are indispensable for resolving this issue.

#### IV. CONCLUSIONS

To conclude, we have investigated both static and dynamic spin susceptibility of  $\text{KNaCuP}_2\text{O}_7$ . Our thermodynamic data are consistent with the theoretical results of a 1D  $S = \frac{1}{2}$  AFHC model down to 1.8 K. Further, we have tested the one-dimensional theory by probing spin transport using zero- and longitudinal-field  $\mu\text{SR}$ . Temperature dependence of the muon spin relaxation rate shows a thermal crossover from diffusive to ballistic spin transport through 30 K. This is contrasted by field-dependent  $\mu\text{SR}$ , which lacks either diffusive or ballistic behaviors. We call for future experiments to clarify the seeming inconsistency.

#### ACKNOWLEDGMENTS

G.S.M. humbly acknowledges Professor F. C. Chou for his guidance and valuable suggestions. We acknowledge W. T. Chen for synchrotron experiment. G.S.M. acknowledges support from the Ministry of Science and Technology in Taiwan under Project No. MOST 106-2119-M-002-035-MY3. R.S. acknowledges the financial support provided by the Ministry of Science and Technology in Taiwan under Project No. MOST-110-2112-M-001-065-MY3 and Academia Sinica budget of AS-iMATE-111-12. The work at SKKU is supported by the National Research Foundation (NRF) of Korea (Grants No. 2020R1A2C3012367 and No. 2020R1A5A1016518).

- [1] E. Ising, *Z. Phys.* **31**, 253 (1925).
- [2] H. Bethe, *Z. Phys.* **71**, 205 (1931).
- [3] T. Giannetti, *Quantum Physics in One Dimension*, Vol. 121 (Clarendon Press, Oxford, UK, 2003).
- [4] N. D. Mermin and H. Wagner, *Phys. Rev. Lett.* **17**, 1133 (1966).
- [5] B. Lake, D. Alan Tennant, C. D. Frost, and S. E. Nagler, *Nat. Mater.* **4**, 329 (2005).
- [6] S. Tomonaga, *Prog. Theor. Phys.* **5**, 544 (1950); J. M. Luttinger, *J. Math. Phys.* **4**, 1154 (1963); D. C. Mattis and E. H. Lieb, *ibid.* **6**, 304 (1965).
- [7] F. D. M. Haldane, *Phys. Rev. Lett.* **45**, 1358 (1980).
- [8] O. A. Castro-Alvaredo, B. Doyon, and T. Yoshimura, *Phys. Rev. X* **6**, 041065 (2016).
- [9] V. B. Bulchandani, R. Vasseur, C. Karrasch, and J. E. Moore, *Phys. Rev. B* **97**, 045407 (2018).
- [10] M. Ljubotina, M. Žnidarič, and T. Prosen, *Phys. Rev. Lett.* **122**, 210602 (2019).
- [11] J. De Nardis, M. Medenjak, C. Karrasch, and E. Ilievski, *Phys. Rev. Lett.* **123**, 186601 (2019).
- [12] J. De Nardis, M. Medenjak, C. Karrasch, and E. Ilievski, *Phys. Rev. Lett.* **124**, 210605 (2020).
- [13] M. Dupont and J. E. Moor, *Phys. Rev. B* **101**, 121106(R) (2020).
- [14] J. Sirker, R. G. Pereira, and I. Affleck, *Phys. Rev. Lett.* **103**, 216602 (2009).
- [15] J. Sirker, R. G. Pereira, and I. Affleck, *Phys. Rev. B* **83**, 035115 (2011).

- [16] M. Hase, I. Terasaki, and K. Uchinokura, *Phys. Rev. Lett.* **70**, 3651 (1993).
- [17] N. Motoyama, H. Eisaki, and S. Uchida, *Phys. Rev. Lett.* **76**, 3212 (1996).
- [18] N. Büttgen, P. Kuhns, A. Prokofiev, A. P. Reyes, and L. E. Svistov, *Phys. Rev. B* **85**, 214421 (2012).
- [19] T. Masuda, A. Zheludev, A. Bush, M. Markina, and A. Vasiliev, *Phys. Rev. Lett.* **92**, 177201 (2004).
- [20] K.-Y. Choi, S. A. Zvyagin, G. Cao, and P. Lemmens, *Phys. Rev. B* **69**, 104421 (2004).
- [21] N. Fujiwara, H. Yasuoka, M. Isobe, Y. Ueda, and S. Maegawa, *Phys. Rev. B* **55**, R11945 (1997).
- [22] T. T. Tran, C. A. Pocs, Y. Zhang, M. J. Winiarski, J. Sun, M. Lee, and T. M. McQueen, *Phys. Rev. B* **101**, 235107 (2020).
- [23] A. A. Belik, M. Azuma, and M. Takano, *J. Solid State Chem.* **177**, 883 (2004).
- [24] M. D. Johannes, J. Richter, S.-L. Drechsler, and H. Rosner, *Phys. Rev. B* **74**, 174435 (2006).
- [25] A. A. Belik, M. Azuma, and M. Takano, *Inorg. Chem.* **42**, 8572 (2003).
- [26] R. Nath, A. V. Mahajan, N. Büttgen, C. Kegler, A. Loidl, and J. Bobroff, *Phys. Rev. B* **71**, 174436 (2005).
- [27] R. Nath, D. Kasinathan, H. Rosner, M. Baenitz, and C. Geibel, *Phys. Rev. B* **77**, 134451 (2008).
- [28] S. Lebernegg, A. A. Tsirlin, O. Janson, R. Nath, J. Sichelschmidt, Y. Skourski, G. Amthauer, and H. Rosner, *Phys. Rev. B* **84**, 174436 (2011).
- [29] I. Fitouri and H. Boughzala, *Acta Cryst. E* **74**, 109 (2018).
- [30] S. Guchhait, Q.-P. Ding, M. Sahoo, A. Giri, S. Maji, Y. Furukawa, and R. Nath, *Phys. Rev. B* **103**, 224415 (2021).
- [31] A. Suter and B. M. Wojek, *Phys. Proc.* **30**, 69 (2012).
- [32] D. C. Johnston, R. K. Kremer, M. Troyer, X. Wang, A. Klümper, S. L. Bud'ko, A. F. Panchula, and P. C. Canfield, *Phys. Rev. B* **61**, 9558 (2000).
- [33] A. Yaouanc and P. Dalmas de Rotier, *Muon Spin Rotation, Relaxation, and Resonance: Applications to Condensed Matter* (Oxford University Press, Oxford, UK, 2011).
- [34] S. Sachdev, *Phys. Rev. B* **50**, 13006 (1994).
- [35] O. A. Starykh, R. P. P. Singh, and A. W. Sandvik, *Phys. Rev. Lett.* **78**, 539 (1997).
- [36] L. F. Pratt, S. J. Blundell, T. Lancaster, C. Baines, and S. Takagi, *Phys. Rev. Lett.* **96**, 247203 (2006).
- [37] R. S. Hayano, Y. J. Uemura, J. Imazato, N. Nishida, T. Yamazaki, and R. Kubo, *Phys. Rev. B* **20**, 850 (1979).
- [38] T. Lancaster, P. J. Baker, F. L. Pratt, S. J. Blundell, W. Hayes, and D. Prabhakaran, *Phys. Rev. B* **85**, 184404 (2012).
- [39] H. Maeter, A. A. Zvyagin, H. Luetkens, G. Pascua, Z. Shermadini, R. Saint-Martin, A. Revcolevschi, C. Hess, B. Büchner, and H.-H. Klauss, *J. Phys.: Condens. Matter* **25**, 365601 (2013).
- [40] K. R. Thurber, A. W. Hunt, T. Imai, and F. C. Chou, *Phys. Rev. Lett.* **87**, 247202 (2001).
- [41] M. Kardar, G. Parisi, and Y.-C. Zhang, *Phys. Rev. Lett.* **56**, 889 (1986).
- [42] A. Scheie, N. E. Sherman, M. Dupont, S. E. Nagler, M. B. Stone, G. E. Granroth, J. E. Moore, and D. A. Tennant, *Nat. Phys.* **17**, 726 (2021).